JOURNAL OF THE AMERICAN CHEMICAL SOCIETY
Article
pubs.acs.org/JACS

Synthesis and Characterization of Patronite Form of Vanadium Sulfide on Graphitic Layer

Chandra Sekhar Rout,[†,‡] Byeong-Hwan Kim,[†,‡] Xiaodong Xu,[†] Jieun Yang,[†] Hu Young Jeong,[†,⊥] Dorj Odkhuu,[†] Noejung Park,[†,∥] Jaephil Cho,*[,†] and Hyeon Suk Shin*[,†]

[†]Interdisciplinary School of Green Energy, Low Dimensional Carbon Materials Center and UNIST Central Research Facilities, UNIST (Ulsan National Institute of Science and Technology), UNIST-gil 50, Ulsan 689-798, Republic of Korea

Supporting Information

ABSTRACT: With the exploding interest in transition metal chalcogenides, sulfide minerals containing the dianion S_2^{2-}, such as pyrite (FeS_2), cattierite (CoS_2), and vaesite (NiS_2), have recently attracted much attention for potential applications in energy conversion and storage devices. However, the synthesis of the patronite structure (VS_4, $V^{4+}(S_2^{2-})_2$) and its applications have not yet been clearly demonstrated because of experimental difficulties and the existence of nonstoichiometric phases. Herein, we report the synthesis of VS_4 using a simple, facile hydrothermal method with a graphene oxide (GO) template and the characterization of the resulting material. Tests of various templates such as CNT, pyrene, perylene-3,4,9,10-tetracarboxylic dianhydride (PTCDA), and graphite led us to the conclusion that the graphitic layer plays a role in the nucleation during growth of VS_4. Furthermore, the VS_4/rGO hybrid was proved to be a promising functional material in energy storage devices.

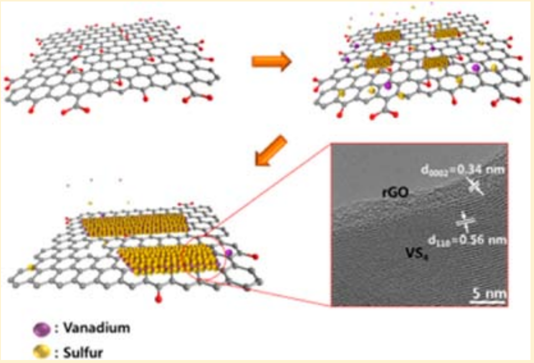

INTRODUCTION

The rapid progress in graphene research has led to intensive exploration of novel two-dimensional (2D) materials.[1−6] In particular, transition-metal dichalcogenides (TMDs), with their layered structures, have received significant attention because they offer many opportunities for fundamental and technological research in a variety of fields, including catalysis, energy storage, sensing, and post-complementary metal oxide semiconductor (CMOS) electronic devices. Recent research trends and the basic properties of TMDs have been well summarized in recent reviews.[1,7]

Among the TMDs, the highly conductive VS_2 is considered to have great potential for applications such as sensors,[8] energy storage devices,[9−11] and spintronics.[12] The VS_2 crystal consists of a metal V layer sandwiched between two S layers, with these triple layers stacking together to form a layered structure with an interlayer spacing of 5.76 Å (Figure 1a). However, since its first reported synthesis as long ago as 1970,[13] the numerous practical difficulties in synthesizing VS_2 have hampered research involving the material. The recent development of a facile synthetic method, along with the growing interest in TMDs, has motivated a renewed effort to carry out novel research on VS_2.[9] On the other hand, VS_4, another vanadium sulfide analogous to VS_2, is a linear-chain compound with two S_2^{2-} moieties between the V centers (Figure 1b).[14] Although the oxidation states of vanadium(IV) in VS_2 and VS_4 are the same, those of the sulfides are different, being an S^{2-} monomer in VS_2 and an S_2^{2-} dimer in VS_4. Since the discovery of the VS_4 mineral (patronite) in 1906[15] and elucidation of its crystallographic structure in 1964,[16] some attempts to synthesize the material have been made; however, evidence of a successful synthesis and characterization of VS_4 have not yet been reported. To date, a systematic study of VS_4, including its synthesis on a large scale, its physicochemical properties, and exploration of its application in different fields, has not been performed owing to experimental difficulties such as the precise control of the partial pressure of S required in the reaction vessel during sulfurization with H_2S.[17,18] Furthermore, the existence of various nonstoichiometric phases of vanadium sulfides with different oxidation states makes the synthesis of a pure form of VS_4 phase extremely difficult.[19,20]

Recently, similar sulfide minerals that include an S_2^{2-} dimer, such as pyrite (FeS_2), cattierite (CoS_2), and vaesite (NiS_2) have been successfully synthesized. These have gained interest owing to their potential applications; for example, FeS_2, with its bandgap of 0.95 eV, has promise as an active layer in photovoltaic devices;[21,22] metallic CoS_2 is a possible catalyst for oxygen reduction reactions and also a potential anode material for Li ion batteries;[23,24] and NiS_2, with its bandgap of 0.3 eV, could be used as a Li storage material.[25,26] Thus, more research is required in the synthesis and exploration of using sulfide minerals with S_2^{2-} dimer as functional materials.

Herein, we report a simple one-step hydrothermal synthesis of VS_4 on a large scale, which is realized by employing a graphene oxide (GO) template. In contrast to metallic VS_2, VS_4

Received: April 1, 2013
Published: May 16, 2013

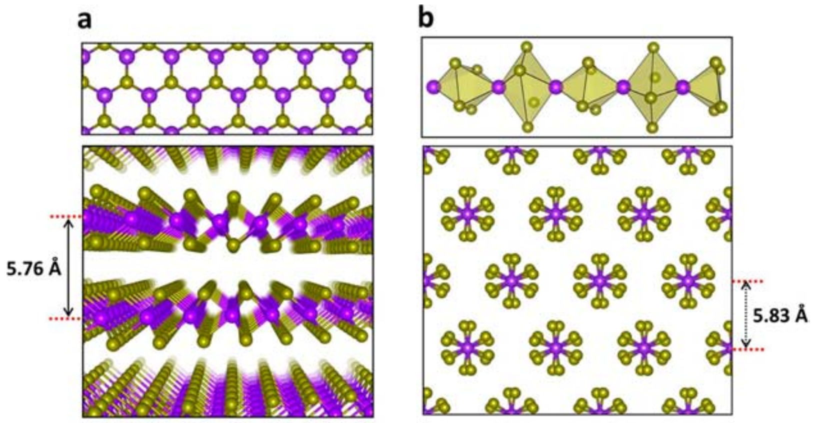

Figure 1. Schematic showing the geometries of VS_2 (a) and VS_4 (b). (a) Top-view image (top) and side-view image (bottom) showing 2D sheets of VS_2. (b) Repeating unit of the 1D chain structure of VS_4 (top) and (b) side-view image of monoclinic VS_4 optimized using DFT. The purple balls are V atoms, and the yellow-green balls are S atoms.

was found by density functional theory (DFT) calculations to be a semiconductor with a bandgap of about 1.0 eV. We here demonstrate that the VS_4/reduced GO (rGO) hybrid is a promising functional material for energy storage devices, in particular, as a Li storage material, owing to its high capacity and fast rate capability, which are superior to those of other metal sulfides as well as VS_2 and rGO alone.

■ RESULTS AND DISCUSSION

Hydrothermal reaction of Na_3VO_4 and C_2H_5NS produced VS_2-layered structures (Figure 2a).[9] Interestingly, the addition of GO into the reaction mixture induced formation of VS_4 instead of VS_2 and the production of a VS_4/rGO hybrid, with the GO being reduced to rGO during the process (Table 1). A schematic of the linear chain VS_4 structure with the V atom bridged to S_2^{2-} is shown in Figure 1b. The scanning electron microscopy (SEM) and transmission electron microscopy (TEM) images shown respectively in b and c of Figure 2 demonstrate the growth of uniformly distributed single-crystalline VS_4 nanostructures on the rGO matrix, with lateral and longitudinal lengths of 50−100 nm and 100−500 nm, respectively. The high-resolution TEM (HRTEM) image in Figure 2d shows the rGO sheets with an interlayer spacing of approximately 0.34 nm ((002) *d*-spacing of graphite), and VS_4 nanostructures with a *d*-spacing of around 0.56 nm, which corresponds to that of the (110) plane of monoclinic phase of VS_4 [PDF No. 072-1294, d (110) = 0.56 nm]. In combination, these results confirm the growth of VS_4 nanostructures on the rGO sheets. Long-range ordering of the stacked rGO layers was not observed, but very thin rGO sheets with 2−5 layers supported the VS_4. The selected area electron diffraction (SAED) pattern of a single nanosheet is well indexed to the single crystalline monoclinic phase of VS_4, as shown in Figure 2e. To determine the stoichiometry of V and S, energy dispersive X-ray spectroscopy (EDX) elemental mapping of the VS_4/rGO hybrids was carried out (Figure 2f), and the results clearly indicate that the ratio of S to V is 4. The presence of C and O in the EDX spectrum is attributed to the rGO. The XRD pattern of the VS_4/rGO hybrid shown in Figure 2g confirms the formation of a monoclinic VS_4 phase with a = 6.78 Å, b = 10.42 Å, and c = 12.11 Å [JCPDS No. 072-1294]. The diffraction peak corresponding to the (110) plane is present at 15.8° (d = 5.61 Å), which is consistent with the *d*-spacing measured in the HRTEM image of Figure 2d. It was found that the optimal experimental conditions for producing highly pure VS_4 were ≥60 mg GO with 1 mM Na_3VO_4 and 5 mM C_2H_5NS in a total volume of 120 mL DI water. A C content of 1.5 wt % was present in the final VS_4/rGO hybrid product by adding the 60 mg GO. At lower GO contents (≤30 mg, ≤0.75 wt %), mixtures of VS_2 and VS_4 phases were formed. (See XRD spectra in Figure S1 in Supporting Information [SI].) This result indicates that the VS_4 phase grows on the GO support, with the VS_2 phase able to be formed within the same reaction mixture but without any support. It is also interesting to note that no peak at approximately 26° in the XRD spectra, which would correspond to rGO sheets, is observed. This confirms that the rGO sheets are extremely thin, as shown in the HRTEM image of Figure 2d.[27,28] X-ray photoelectron spectroscopy (XPS) confirmed the reduction of V^{5+} to V^{4+} and GO to rGO.[29,30] The XPS C 1s, V 2p, and S 2p core-level spectra are shown in Figure 2h. The C 1s peak centered at 284.4 eV was ascribed to the presence of nonoxygenated sp^2 C in the basal plane of rGO, and the fitted peak observed at the higher binding energy indicates the presence of a trace amount of oxygen-containing functional groups.[29] The S 2p core level analysis demonstrates the existence of the S_2^{2-} species in the VS_4/rGO hybrids, and the peaks at 162.4 and 163.5 eV can be indexed to S $2p_{3/2}$ and S $2p_{1/2}$, respectively, for the S_2^{2-} dimer. It has previously been shown that the binding energy of S $2p_{3/2}$ for the S_2^{2-} dimer in FeS_2 and NiS_2 appears between 162.3 and 162.8 eV, but that for S^{2-} appears around 161 eV.[22,31−33] The binding energy of S $2p_{3/2}$ for VS_2 (S^{2-}) synthesized in this study appears at 160.6 eV (Figure S2 in SI). The peaks at 515.6 and 523.1 eV are attributed to V $2p_{3/2}$ and V $2p_{1/2}$, which are characteristic of V^{4+} rather than V^{5+} (V 2p peak positions for V^{5+} are at 517.2 ± 0.1 and 524.6 ± 0.1 eV),[30] confirming the formation of V^{4+} $(S_2^{2-})_2$ in the VS_4/rGO hybrids.

To investigate the electronic and geometric structures of VS_2 and VS_4, DFT calculations were performed using the Vienna Ab Initio Simulation Package (VASP).[34−37] The plane-wave basis set with an energy cutoff of 400 eV and the PBE-type gradient-corrected exchange-correlation potential were employed.[38] The projected density of states (PDOSs) onto V and S for optimized stacks of 2D VS_2, are presented in Figure 3a. The PDOSs near the Fermi level indicate that VS_2 has metallic nature with the large polarization in the electron spins of the 3d electrons of V. The bulk VS_4 structures were optimized using the known patronite crystal structure shown in

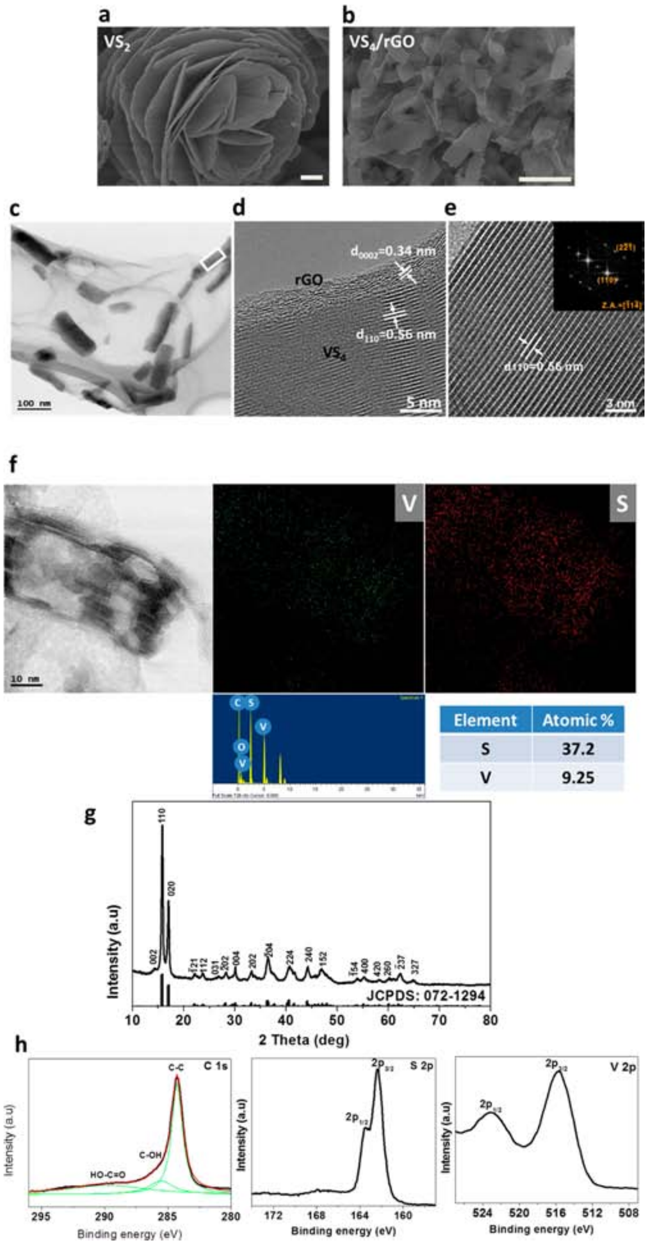

Figure 2. SEM images of a (a) VS_2 flowerlike structure and (b) VS_4/rGO hybrid (scale bar is 500 nm). (c) Low-magnification bright-field TEM image of VS_4/rGO hybrid. (d) Enlarged HRTEM image of the region marked with a white rectangle in (c). The rGO sheets with an interlayer distance of 0.34 nm can be clearly distinguished. (e) Higher-magnification HRTEM image of VS_4, showing the *d*-spacing of 0.56 nm in the (110) plane. The fast-Fourier transform (FFT) pattern shown in the inset is consistent with the monoclinic VS_4 phase (a = 6.78 Å, b = 10.42 Å, c = 12.11 Å) with a [−11−4] zone axis. (f) TEM image corresponding to EDX elemental mapping of V and S, EDX spectrum and table showing elemental composition. The atomic ratio of S and V is 4, confirming the stoichiometry of VS_4. (g) XRD pattern of VS_4/rGO hybrid is consistent with known monoclinic VS_4 [JCPDS No. 072-1294]. (h) XPS spectra showing the C 1s, S 2p, and V 2p core levels for the VS_4/rGO hybrid.

Table 1. Vanadium Sulfide Products Obtained in the Hydrothermal Reactions with Na_3VO_4, C_2H_5NS, and Various Precursors of GO, CNT-COOH, Pyrene-COOH, PTCDA, graphite, TiO_2, and Au Nanoparticles

precursors	$\xrightarrow[160\ ^\circ\mathrm{C}/24\ \mathrm{h}]{\text{hydrothermal rxn}}$	products (vanadium sulfide)
Na_3VO_4 + C_2H_5NS		VS_2
Na_3VO_4 + C_2H_5NS + GO		VS_4
Na_3VO_4 + C_2H_5NS + CNTs		VS_4
Na_3VO_4 + C_2H_5NS + pyrene-COOH		VS_2
Na_3VO_4 + C_2H_5NS + PTCDA		VS_4
Na_3VO_4 + C_2H_5NS + graphite		VS_4 and VS_2
Na_3VO_4 + C_2H_5NS + TiO_2 particles		VS_2
Na_3VO_4 + C_2H_5NS + Au nanoparticles		VS_2

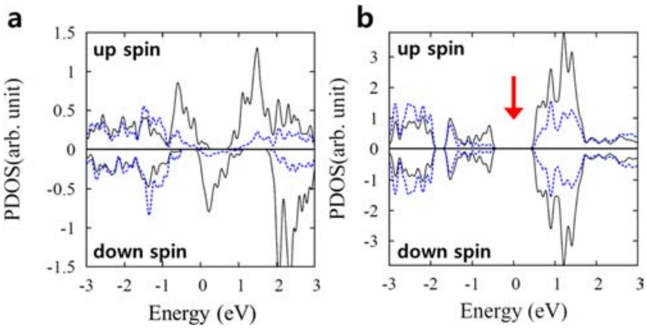

Figure 3. (a) PDOS for V (solid line) and S (dashed line) of VS_2. (b) PDOS for V (solid line) and S (dashed line) of VS_4. Upper and lower panels represent spin-up and spin-down states, respectively.

Figure 1b.[16,39] V atoms are surrounded by S rectangles, constituting a one-dimensional chain structure (inset of Figure 1b). The bulk VS_4 is the aggregation of VS_4 chains through the interchain dispersion forces. VS_4 develops a finite bandgap, as shown in Figure 3b, with the DFT gap found to be approximately 1.0 eV. Considering that DFT calculations underestimate the bandgap, this result is consistent with the observation of the absorption edge at 1.35 eV, which was determined from the UV/vis spectrum of the VS_4/rGO hybrid dispersed in formamide (Figure S3 in SI).

To investigate the process of VS_4 formation on the GO sheets, the hydrothermal reactions were carried out at various reaction times from 30 min to 24 h, and the products were characterized using XRD and XPS (Figure S4 in SI). The XRD spectra indicate that the pattern corresponding to the VS_4 phase was observed at reaction times over 3 h, whereas only broad peaks around 13° (d = 6.5 Å) were observed prior to this time. It is assumed that these broad peaks correspond to partially reduced GO layers and intercalation of decomposed species of precursors (see C 1s, S 2p, and V 2p binding energies in XPS spectra of Figure S4 in SI). However, the absence of the broad peaks after 3 h of reaction indicates a lack of GO stacking but the presence of very thin GO layers, as demonstrated previously. Thus, it is speculated that the nucleation of VS_4 on GO sheets with adsorption of decomposed precursors started after approximately 2 h, with subsequent VS_4 growth and inhibition of the restacking of GO sheets.

The role of GO in VS_4 growth during the hydrothermal reaction was estimated by carrying out the hydrothermal reactions in the presence of carboxyl-functionalized carbon nanotubes (CNT-COOH), pyrene modified with carboxylic acids (pyrene-COOH), perylene-3,4,9,10-tetracarboxylic dianhydride (PTCDA), graphite, and Au and TiO_2 nanoparticles. CNT-COOH induced synthesis of VS_4 in a manner identical to that of the GO sheets (Table 1 and Figure S5 in SI). However, when pyrene-COOH was used, only VS_2 sheets were

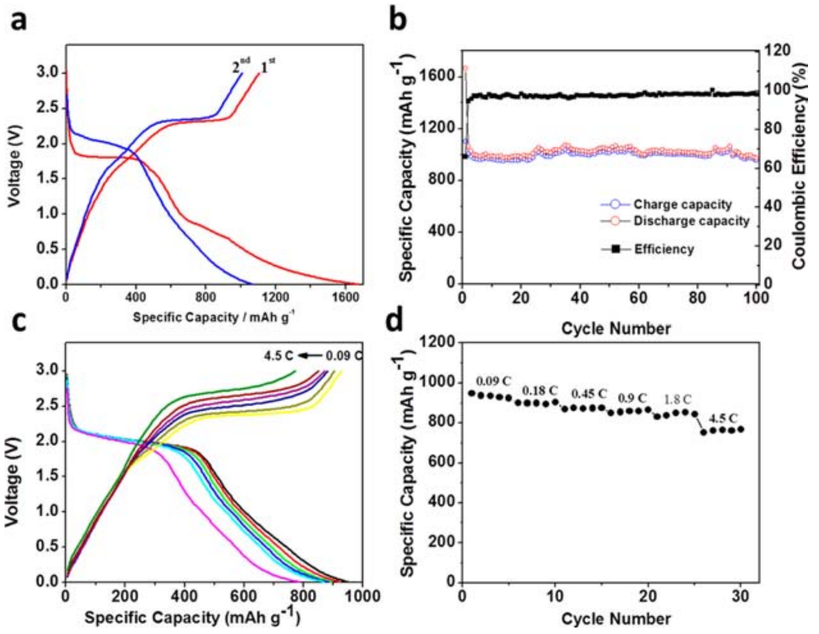

Figure 4. (a) First and second discharge−charge voltage profiles of VS_4/rGO hybrid at a rate of 0.1 C in a coin-type Li cell (2016R) at 23 °C. (b) Cycling performance of VS_4/rGO at 0.1 C. (c) Voltage profiles of VS_4/rGO at different current rates. (D) Rate performance with increasing charge rate from 0.09 to 4.5 C. The discharge rate is fixed at 0.09 C (1 C = 1000 mA g^{-1}).

synthesized, with no conversion to the VS_4 phase (Figure S6 in SI). On the other hand, PTCDA, which has a slightly greater graphitic (or sp^2) domain than pyrene, induced mixtures of VS_4, an unknown product, and unreacted PTCDA (Figure S7 in SI). It should be noted that CNT-COOH and pyrene-COOH are soluble in water, whereas PTCDA only forms a dispersed phase. In addition, the hydrothermal reaction with graphite showed a small amount of VS_4, with VS_2 as the major product, indicating that graphite contributed to the partial conversion to VS_4 phase (Figure S8 in SI). It is assumed that the contribution of the graphite surface to the growth of VS_4 occurred because graphite is thick, but its lack of solubility in water inhibited complete conversion to VS_4. From the results of hydrothermal reactions with these alternative components to GO, it is speculated that the graphitic domain acts as a template or support for nucleation and growth of VS_4. The water solubility of the GO and CNT-COOH, in addition to their large graphitic regions, induced synthesis of the pure VS_4 phase. However, although pyrene-COOH was water-soluble, it did not provide a large enough area as a template for nucleation and growth, and conversely, the slightly larger PTCDA contributed to growth of VS_4 even though its solubility was poor. For reference, the same hydrothermal reaction with TiO_2 and Au nanoparticles did not induce conversion of VS_2 to VS_4, but produced only the VS_2 phase (Figures S9 and S10 in SI). Thus, it was concluded that water-soluble templates with a larger graphitic domain size than that in PTCDA were necessary for the growth of VS_4.

Indeed, rGO has been used as a template for the morphology-controlled synthesis of various nanomaterials, including metals, metal oxides, and transition-metal chalcogenides.[40−42] It appears that rGO sheets contribute to the controlled nucleation and growth, affording optimal chemical interactions and bonding between the nanomaterial and the rGO. For example, Wang et al. demonstrated the synthesis of $LiMn_{0.75}Fe_{0.25}PO_4$ nanorods anchored on rGO by using a hydrothermal process, whereas they observed the formation of irregularly shaped $LiMn_{0.75}Fe_{0.25}PO_4$ particles in the absence of the rGO.[40] Deng et al. observed the formation of Cu_2O nanowire mesocrystals in the presence of GO, whereas only Cu_2O nanowires were formed without it under hydrothermal conditions.[41] In this case, GO serves as a crystal growth modifier to promote the initial growth of agglomerated amorphous spherical Cu_2O nanoparticles. However, GO in our result induced a change of chemical composition, which is different from the above morphology control.

In order to demonstrate the potential of the synthesized VS_4/rGO hybrid, it was applied as a Li storage material. Figure 4a shows the first and second discharge−charge voltage profiles of a 3% VS_4/rGO composite within a cutoff voltage window of 0.01−3.0 V at a current rate of 0.1 C (1 C = 1000 mA g^{-1}) in a coin-type Li half-cell (2016R). The initial discharge and charge capacities of VS_4/rGO were found to be 1669 and 1105 mA h g^{-1}, respectively, showing a Coulombic efficiency of 66%. This low efficiency is due to the inevitable decomposition of the electrolyte and the formation of a solid electrolyte interface (SEI), which is common in transition-metal oxide and sulfide-based anode materials.[43] The discharge and charge capacities were found to be 1066 and 1009 mA h g^{-1}, respectively, during the second cycle, with an improved Coulombic efficiency of 95%. Figure 4b demonstrates the good cycling performance of the as-prepared VS_4/GO composite. After 100 cycles at 0.1 C, the material still retained a high charge capacity of 954 mA h g^{-1}, which is 95% of the initial capacity. Furthermore, its Coulombic efficiency was maintained at >97% after the third cycle. Parts c and d of Figure 4 show the rate performance of VS_4/GO composite at different charge rates. The VS_4/rGO hybrid retained 83% capacity when the current rate was increased by a factor of 50, from 924 mA h g^{-1} at 0.09 C to 766 mA h g^{-1} at 4.5 C. Such an impressive electrochemical performance of the VS_4/rGO could be attributed to the retention of the electrical conductivity network of VS_4 owing to the rGO dispersed between the VS_4 structures.[44−46] This is because VS_2 electrode in the absence of rGO would become pulverized and lose electrical integrity owing to the large volume change during discharge−charge cycling, which are also common phenomena occurring in high-capacity anode material.[47] The possibility that the rGO itself contributed directly to the electrochemical performance was excluded because the content of rGO was just 3 wt %. Furthermore, as control experiments, rGO (prepared using the same hydrothermal reaction) or VS_2 sheets were tested individually and were found to show poor electrochemical performance (Figures S11 and S12 in SI). Therefore, the VS_4/rGO hybrid demonstrated great potential as a new anode material for Li batteries. Further research, including the optimization and working mechanism of Li batteries employing this material, is under study.

■ CONCLUSION

In conclusion, we have synthesized and characterized a VS_4-based hybrid material on a large scale. The structure and growth of the hybrid, along with its application as an anode material for Li batteries was demonstrated. Initial discharge and charge capacities of the VS_4/rGO were found to be 1669 and 1105 mA h g^{-1}, respectively, and good cycling performance, with the retention of a high charge capacity of 954 mA h g^{-1} after 100 cycles at 0.1 C, was also shown. Furthermore, we have systematically studied the mechanism of growth of the VS_4 phase in the presence of GO. This approach sheds light on the structures and properties of other metal sulfides, in addition to VS_4, and opens up numerous possibilities for their future use.

■ EXPERIMENTAL SECTION

Synthesis of GO Solution. GO was prepared from natural graphite powder by the modified Hummers' method.[48] Two grams of graphite powder (SP-1, Bay carbon), 1 g of $K_2S_2O_8$ (Sigma Aldrich, ≥99.0%), and 1 g P_2O_5 (Sigma Aldrich, 99.99%) were taken in 8 mL of H_2SO_4 (Merck Chemicals, 98%) and heated at 80 °C. The resultant dark-blue mixture was allowed to cool to room temperature; after reaching room temperature it was stirred for 6 h. The mixture was then filtered, washed, and dried in vacuum at ambient temperature overnight. This preoxidized graphite was then subjected to oxidation. The preoxidized graphite powder was put into 46 mL of H_2SO_4 at 0 °C, and 6 g of $KMnO_4$ (Sigma Aldrich, ≥99.0%) was added gradually. The mixture was then stirred at 35 °C for 2 h, and 92 mL of distilled water was added. In 15 min, the reaction was terminated by the addition of 280 mL of distilled water and 5 mL of H_2O_2 (SAMCHUN pure chemical, 34.5% extra pure) solution, and then the color of the mixture changed to yellow. The mixture was filtered and washed with 500 mL of HCl (SAMCHUN pure chemical, 10 wt %) solution. The resulting graphite oxide was suspended in 200 mL of distilled water again, followed by dialysis (dialysis membrane: Spectrum Laboratories, MWCO-12−14,000) to remove excess HCl. The graphite oxide is exfoliated to give ∼5 mg/mL GO solution by a high-pressure homogenizer at 15,000 psi. After exfoliation, the solution was centrifuged at 3500 rpm for 10 min to remove the nonexfoliated graphite oxide, and the top supernatant GO solution was used for the hydrothermal reaction.

Functionalization of CNTs. CNTs (Cheaptubes, >95%, outer diameter: 30−50 nm, length: 10−20 μm) were treated with a mixture of concentrated sulfuric acid (95%) and nitric acid (60%) (3:1), followed by ultrasonication at 50 °C. Next, the product was diluted with water and kept for overnight. Lastly, it was filtered and dried in vacuum to get CNTs functionalized with carboxylic acid.

VS_2 Sheets. VS_2 sheets were synthesized by a one-step hydrothermal reaction. In a typical experiment, 1.65 g of sodium orthovanadate (1 mM Na_3VO_4, Sigma-Aldrich, 99.98%) and 3.37 g of thioacetamide (5 mM C_2H_5NS, Sigma-Aldrich, ≥ 99%) were dissolved in 120 mL of DI water and stirred for 1 h at room temperature by using a magnetic stirrer. The solution was transferred to a 150-mL Teflon-lined stainless steel autoclave, heated up to 160 °C, and kept for 24 h. After cooling naturally, the product was filtered, washed with DI water, and dried in vacuum at 60 °C for 6 h.

VS_4/rGO Hybrids. VS_4/rGO hybrids with different concentrations of rGO were synthesized by the same hydrothermal reaction condition as that for VS_2 sheets. A GO solution of 5 mg/mL was added to the mixture of sodium orthovanadate and thioacetamide, and a total volume of the solution was adjusted to 120 mL for all reactions. The solution was transferred to a 150-mL Teflon-lined stainless steel autoclave, heated up to 160 °C, and kept for 24 h. After cooling naturally, the product was filtered, washed with DI water, and dried in vacuum at 60 °C for 6 h. During the hydrothermal process, VS_4 were formed on GO, and GO was transformed to rGO. VS_4/rGO hybrids with different amounts of rGO were obtained by adding different volumes of 5 mg/mL GO solution to the above mixtures of sodium orthovanadate and thioacetamide: 2.4, 6, 12, 24, 48, and 96 mL. The actual amounts of rGO in the final VS_4/rGO hybrids products were estimated from carbon contents (wt %) by elemental analysis: 0.3 wt % for 2.4 mL, 0.75 wt % for 6 mL, 1.5 wt % for 12 mL, 3 wt % for 24 mL, 6 wt % for 48 mL, and 12 wt % for 96 mL of 5 mg/mL GO solution.

VS_4/CNTs Hybrids. VS_4/CNTs hybrids with different concentrations of CNTs were synthesized by following the same hydrothermal reaction condition as that for VS_4/rGO. A functionalized CNTs solution of 30 mg/ML was added to the mixture of sodium orthovanadate and thioacetamide, and then a total volume of the solution was adjusted to 120 mL for all reactions. The solution was transferred to a 150-mL Teflon-lined stainless steel autoclave, heated up to 160 °C, and kept for 24 h. After cooling naturally, the product was filtered, washed with DI water, and dried in vacuum at 60 °C for 6 h. VS_4/CNTs hybrids with different amounts of CNTs were obtained by adding different volumes of 30 mg/mL CNTs solution to the above mixture of sodium orthovanadate and thioacetamide: 0.04, 0.12, 0.3, 0.6, 2.4, and 9.6 mL. The actual amounts of CNTs in the final VS_4/CNTs hybrids were estimated from carbon contents (wt %) by elemental analysis: 0.1 wt % for 0.04 mL, 0.3 wt % for 0.12 mL, 0.75 wt % for 0.3 mL, 1.5 wt % for 0.6 mL, 6 wt % for 2.4 mL, and 24 wt % for 9.6 mL of 30 mg/mL CNTs solution.

Hydrothermal Reactions with Various Precursors. After a precursor was added together with sodium orthovanadate and thioacetamide in 120 mL of DI water, the same hydrothermal reaction for VS_2 sheets was carried out. Tested precursors were 0.26 g of pyrene-COOH (Sigma-Aldrich, ≥98%), 0.39 g of PTCDA (Sigma-Aldrich, ≥98%), 0.12 g of graphite (SP-1, Bay carbon), 0.12 g of TiO_2 (Sigma-Aldrich, >95%, particle size: 20 nm), and 25 mL of Au nanoparticles (Sigma-Aldrich, particle size: 10 nm, stabilized suspension in citrate buffer).

Characterization. The samples were characterized with X-ray diffraction ((Rigaku RU-200 diffractometer) equipped with Ni-filtered Cu Kα radiation (40 kV, 100 mA, λ = 0.15418 nm), high-resolution transmission electron microscopy (HRTEM, JEOL JEM-2100 F with probe-Cs corrector, 200 kV), field emission scanning electron microscopy (Hitachi, S4800), micro Raman spectrometer (Alpha 300s, WITec GmbH) with a laser excitation wavelength of 532 nm, UV−vis micro-spectrophotometer (Agilent, Cary 5000), FTIR (Varian, 670-IR), and X-ray photoelectron spectroscopy (K-alpha, Thermo Fisher) with monochromatic Al Kα radiation as the X-ray source.

Electrochemical Measurements. The anodes were made of VS_4/rGO, rGO, or VS_2, Ketjen Black, and polyvinylidone fluoride (PVDF) binder (LG Chem) in a weight ratio of 80:10:10. The coin-type half cells (2016R) were assembled in an Ar-filled glovebox, using lithium metal foil as the counterelectrode, microporous polyethylene as the separator, and 1.1 M $LiPF_6$ in ethylene carbonate/diethylene carbonate (EC/DEC, 1:1 in volume ratio, Panax Starlyte, Korea) as the electrolyte. The loading amount of the electrode material was measured as >1 mg cm^{-2}. The cell tests were performed with a WBCS3000 automatic battery cycler system, and the capacity was estimated only on the basis of the active materials. All measurements were carried out at room temperature.

ASSOCIATED CONTENT

Supporting Information

XRD and XPS spectra for VS_2 and VS_4/rGO, UV−vis−NIR spectra for VS_4/rGO, SEM images and XRD spectra for VS_4/CNT, VS_4/pyrene, VS_4/PTCDA, VS_4/graphite, VS_4/TiO_2 nanoparticles and VS_4/Au nanoparticles, and the initial discharge−charge voltage profiles of VS_2 and rGO. This material is available free of charge via the Internet at http://pubs.acs.org.

AUTHOR INFORMATION

Corresponding Author

shin@unist.ac.kr (H.S.S.); jpcho@unist.ac.kr (J.C.)

Present Addresses

[∥]Interdisciplinary School of Green Energy and Low Dimensional Carbon Materials Center, UNIST (Ulsan National Institute of Science and Technology), UNIST-gil 50, Ulsan 689-798, Republic of Korea.

[⊥]UNIST Central Research Facilities, UNIST (Ulsan National Institute of Science and Technology), UNIST-gil 50, Ulsan 689-798, Republic of Korea.

Author Contributions

[‡]C.S.R. and B.-H.K. contributed equally.

Notes

The authors declare no competing financial interest.

ACKNOWLEDGMENTS

This work was supported by the WCU (World Class University) Program (R31-2008-000-20012-0), the Basic Science Research Program (2011-0013601), Grant from the Center for Advanced Soft Electronics (Code No. 2011-0031630) under the Global Frontier Research Program, and the Converging Research Center Program (2012K001251) through the National Research Foundation funded by MEST of Korea.

REFERENCES

(1) Wang, Q. H.; Kalantar-Zadeh, K.; Kis, A.; Coleman, J. N.; Strano, M. S. *Nat. Nanotechnol.* **2012**, *7*, 699−712.

(2) Cao, T.; Wang, G.; Han, W.; Ye, H.; Zhu, C.; Shi, J.; Niu, Q.; Tan, P.; Wang, E.; Feng, L. *Nat. Commun.* **2012**, *3*, 887.

(3) Zeng, H.; Dai, J.; Yao, W.; Xiao, D.; Cui, X. *Nat. Nanotechnol.* **2012**, *7*, 490−493.

(4) Mak, K. F.; He, K.; Shan, J.; Heinz, T. F. *Nat. Nanotechnol.* **2012**, *7*, 494−498.

(5) Eda, G.; Yamaguchi, H.; Voiry, D.; Fujita, T.; Chen, M.; Chhowalla, M. *Nano Lett.* **2011**, *11*, 5111−5116.

(6) Eda, G.; Fujita, T.; Yamaguchi, H.; Voiry, D.; Chen, M. W.; Chhowalla, M. *ACS Nano* **2012**, *6*, 7311−7317.

(7) Chhowalla, M.; Shin, H. S.; Eda, G.; Li, L.-J.; Loh, K. P.; Zhang, H. *Nat. Chem.* **2013**, *5*, 263−275.

(8) Feng, J.; Peng, L.; Wu, C.; Sun, X.; Hu, S.; Lin, C.; Dai, J.; Yang, J.; Xie, Y. *Adv. Mater.* **2012**, *24*, 1969−1974.

(9) Feng, J.; Sun, X.; Wu, C.; Peng, L.; Lin, C.; Hu, S.; Yang, J.; Xie, Y. *J. Am. Chem. Soc.* **2011**, *133*, 17832−17838.

(10) Therese, H. A.; Rocker, F.; Reiber, A.; Li, J.; Stepputat, M.; Glasser, G.; Kolb, U.; Tremel, W. *Angew. Chem., Int. Ed.* **2005**, *44*, 262−265.

(11) Murugan, A. V.; Quintin, M.; Delville, M.-H.; Campet, G.; Vijayamohanan, K. *J. Mater. Chem.* **2005**, *15*, 902−909.

(12) Ma, Y.; Dai, Y.; Guo, M.; Niu, C.; Zhu, Y.; Huang, B. *ACS Nano* **2012**, *6*, 1695−1701.

(13) Murphy, D. W.; Cros, C.; Di Slavo, F. J.; Waszczak, J. V. *Inorg. Chem.* **1977**, *16*, 3027−3031.

(14) Vaughan, D. J.; Craig, J. R. *Mineral Chemistry of Metal Sulfides*; Cambridge University Press: Cambridge, 1978.

(15) Hillebrand, W. F. *J. Am. Chem. Soc.* **1907**, *29*, 1019−1029.

(16) Patronite Mineral Data. Mineralogy Database: http://www.webmineral.com/data/Patronite.shtml.

(17) Yokoyama, M.; Yoshimura, M.; Wakihara, M.; Somiya, S.; Taniguchi, M. *J. Solid State Chem.* **1985**, *60*, 182−187.

(18) Onada, M. N.; Yamaoka, S.; Yukino, K.; Kato, K.; Kawada, I. A. *J. Less-Common Met.* **1976**, *24*, 341−344.

(19) Taniguchi, M.; Wakihara, M.; Shirai, Y. *Z. Anorg. Allg. Chem.* **1980**, *461*, 234−240.

(20) Murugesan, T.; Ramesh, S.; Gopalkrishnan, J.; Rao, C. N. R. *J. Solid State Chem.* **1982**, *44*, 119−125.

(21) Puthussery, J.; Seefeld, S.; Berry, N.; Gibbs, M.; Law, M. *J. Am. Chem. Soc.* **2011**, *133*, 716−719.

(22) Morrish, R.; Silverstein, R.; Wolden, C. A. *J. Am. Chem. Soc.* **2012**, *134*, 17854−17857.

(23) Jirkovsky, J. S.; Björling, A.; Ahlberg, E. *J. Phys. Chem. C* **2012**, *116*, 24436−24444.

(24) Wang, Q.; Jiao, L.; Han, Y.; Du, H.; Peng, W.; Huan, Q.; Song, D.; Si, Y.; Wang, Y.; Yuan, H. *J. Phys. Chem. C* **2011**, *115*, 8300−8304.

(25) Yang, S.-L.; Yao, H.-B.; Gao, M.-G.; Yu, S.-H. *CrystEngComm* **2009**, *11*, 1383−1390.

(26) Takeuchi, T.; Sakaebe, H.; Kageyama, H.; Sakai, T.; Tatsumi, K. *J. Electrochem. Soc.* **2008**, *155*, A679−A684.

(27) Chang, K.; Chen, W. *Chem. Commun.* **2011**, *47*, 4252−4254.

(28) Wang, B.; Park, J.; Su, D.; Wang, C.; Ahn, H.; Wang, G. *J. Mater. Chem.* **2012**, *22*, 15750−15756.

(29) Li, Y.; Wang, H.; Xie, L.; Liang, Y.; Hong, G.; Dai, H. *J. Am. Chem. Soc.* **2011**, *133*, 7296−7299.

(30) Silvermit, G.; Delpa, D.; Poleman, H.; Marin, G. B.; Gryse, R. D. *J. Electron Spectrosc. Relat. Phenom.* **2004**, *135*, 167−175.

(31) Leiro, J. A.; Mattila, S. S.; Laajalehto, K. *Surf. Sci.* **2003**, *547*, 157−161.

(32) Nesbitt, H. W.; Schaufuss, A. G.; Scani, M.; Bancroft, G. M.; Szargan, R. *Am. Minerol.* **2001**, *86*, 318−326.

(33) Sangaletti, L.; Parmigiani, F. *Phys. Rev. B* **1997**, *55*, 9514−9519.

(34) Hohenberg, B.; Kohn, W. *Phys. Rev.* **1964**, *136*, B864−B871.

(35) Kohn, W.; Sham, L. J. *Phys. Rev.* **1965**, *140*, A1133−A1138.

(36) Kresse, G.; Furthmüller, J. *Phys. Rev. B* **1996**, *54*, 11169−11186.

(37) Kresse, G.; Furthmüller, J. *Comput. Mater. Sci.* **1996**, *6*, 15−50.

(38) Perdew, J. P.; Burke, K.; Ernzerhof, M. *Phys. Rev. Lett.* **1996**, *77*, 3865−3868.

(39) Hibble, S.; Walton, R. I.; Pickup, D. M. *J. Chem. Soc., Dalton Trans.* **1996**, 2245−2251.

(40) Wang, H.; Yang, Y.; Liang, Y.; Cui, L.-F.; Casalongue, H. S.; Li, Y.; Hong, G.; Dai, H. *Angew. Chem., Int. Ed.* **2011**, *123*, 7502−7506.

(41) Deng, S.; Tjoa, V.; Fan, H. M.; Tan, H. R.; Sayle, D. C.; Olivo, M.; Mhaisalkar, S.; Wei, S.; Sow, C. H. *J. Am. Chem. Soc.* **2012**, *134*, 4905−4917.

(42) Pak, C.; Lee, D. C. *ACS Appl. Mater. Interfaces* **2012**, *4*, 1021−1029.

(43) Cabana, J.; Monconduit, L.; Larcher, D.; Palacin, M. R. *Adv. Mater.* **2010**, *22*, E170−E192.

(44) Wang, H.; Liang, Y.; Gong, M.; Li, Y.; Chang, W.; Mefford, T.; Zhou, J.; Wang, J.; Regier, T.; Wei, F.; Dia, H. *Nat. Commun.* **2012**, *3*, 917.

(45) Xin, S.; Guo, Y.-G.; Wan, L.-J. *Acc. Chem. Res.* **2012**, *45*, 1759−1769.

(46) Dai, L.; Chang, W.; Baek, J.-B.; Lu, W. *Small* **2012**, *8*, 1130−1166.

(47) Cho, J. *J. Mater. Chem.* **2010**, *20*, 4009−4014.

(48) Kovtyukhova, N. I.; Ollivier, P. J.; Martin, B. R.; Mallouk, T. E.; Chizhik, S. A.; Buzaneva, E. V.; Gorchinskiy, A. D. *Chem. Mater.* **1999**, *11*, 771.